

Article

Study of the Mechanical Properties and Microstructural Response with Laser Shock Peening on 40CrMo Steel

Xiaoming Pan ^{1,*} , Zhiyang Gu ², Hui Qiu ¹, Aixin Feng ¹ and Jing Li ³

¹ College of Mechanical & Electrical Engineering, Wenzhou University, Wenzhou 325035, China; 20190081@wzu.edu.cn (H.Q.); aixfeng@wzu.edu.cn (A.F.)

² Institute of Intelligent Manufacturing, Wenzhou Polytechnic, Wenzhou 325035, China; guzy@mail.nwpu.edu.cn

³ School of Mechanical Engineering and Rail Transit, Changzhou University, Changzhou 213164, China; ljing@cczu.edu.cn

* Correspondence: 00132004@wzu.edu.cn

Abstract: In this work, the purpose of the study was to explore the influence of laser shock peening (LSP) on the mechanical behavior and microstructural response of 40CrMo steel. The residual stress at depth direction and the microstructural evolution of 40CrMo steel specimens without and with LSP treatments were tested by residual stress tester and transmission electron microscopy (TEM). The microhardness at depth direction and the tensile properties at room temperature were measured. Moreover, the effects of LSP on the ability to resist wear of 40CrMo steel were analyzed, and the worn morphologies characteristics were observed by scanning electron microscope (SEM). The results demonstrated that LSP led to the surface residual stress convert from tensile stress to compressive stress, while the surface compressive residual stress tested parallel to the laser path of the specimen subjected to LSP reached -425 MPa. After the LSP process, the average surface microhardness reached 338 HV, which increased by 21.58% than that of the untreated sample. LSP could enhance the strength without losing plasticity significantly, while the average tensile strength reached 1165 MPa, and the fracture elongation reached 13.9%. After a friction and wear test, the mass loss of the sample after LSP treatment reduced by 27.5% compared to the original sample. The increase in dislocation density and the formation of deformation twins generated by LSP played a key role in enhancing the mechanical behavior of 40CrMo steel.

Keywords: laser shock peening; 40CrMo steel; mechanical properties; residual stress; microstructure



Citation: Pan, X.; Gu, Z.; Qiu, H.; Feng, A.; Li, J. Study of the Mechanical Properties and Microstructural Response with Laser Shock Peening on 40CrMo Steel. *Metals* **2022**, *12*, 1034. <https://doi.org/10.3390/met12061034>

Academic Editor: Aleksander Lisiecki

Received: 8 April 2022
Accepted: 7 June 2022
Published: 17 June 2022

Publisher's Note: MDPI stays neutral with regard to jurisdictional claims in published maps and institutional affiliations.



Copyright: © 2022 by the authors. Licensee MDPI, Basel, Switzerland. This article is an open access article distributed under the terms and conditions of the Creative Commons Attribution (CC BY) license (<https://creativecommons.org/licenses/by/4.0/>).

1. Introduction

40CrMo steel has been widely employed in manufacturing some extremely critical components such as shafts, gears and bearings due to its high plasticity, as well as high creep strength and high-temperature stability [1,2]. However, 40CrMo steel is generally used in high temperature, cyclic loading, corrosion and other harsh environments, which easily cause fatigue or even breakage [3,4]. Therefore, how to further enhance the mechanical properties of 40CrMo steel has received extensive attention.

For the improvement of the comprehensive mechanical properties of structural steel, some scholars have carried out numerous researches [5,6]. For example, YuyunYang et al. investigated the influence of supersonic fine particle bombardment pretreatment on the mechanical properties of the vacuum carburized 18Cr2Ni4WA. The experimental result suggested that the refined grain-boundaries generated by supersonic fine particle bombardment pretreatment led to higher hardness, and the tribological property results suggested that the weight loss and friction coefficient of vacuum carburized 18Cr2Ni4WA subjected to supersonic fine particle bombardment were the lowest [5]. Junjie Sun obtained lamella structured low-carbon steel with bimodal grain size for potentially enhancing the mechanical properties. In addition, the experimental results showed that the ultrafine grain

contributed to enhancing the strength, while both the bimodal grain size and the lamellar structure contributed to enhancing the reasonable ductility [6].

As a novel surface deformation strengthening technique, laser shock peening (LSP) employs pulsed laser-induced high-pressure shock waves to produce severe plastic deformation for processed materials, and induce the formation of dislocation walls, dislocation cells and other dislocation structures [7–9]. In addition, the dislocation structures are transformed into sub-crystalline or high-angle grain boundaries through the dynamic recrystallization process to refine the material grains, which has been widely used in the field of anti-fatigue manufacturing. For example, Jian Wang et al. studied the effects of multiple LSP impacts on the microstructures and mechanical behavior of 2A14 aluminum alloy, and they found that the enhancement of mechanical behavior was contributed to by the microstructural response generated by LSP [10]. Peng Liu et al. probed the influence of LSP on the friction stir welded joints of 7050-T7451 alloys, and the results showed that LSP effectively improved the hardness and fatigue life of the specimen [11]. Liang Lan characterized microstructural evolutions of Ti-6Al-4V alloy modified via LSP, and found that the grain refined, and the gradient distribution of α phase and compressive residual stress contributed to the increase in strength and ductility [12].

Compared to other deformation strengthening technologies, LSP has the following unique features [13,14]. (1) High pressure, the pressure caused by the laser shock wave can reach several GPa. (2) Ultra-high strain rate, the laser shock wave action time is only tens of nanoseconds. Due to the extremely short action time of the shock wave, the strain rate is 10^4 times higher than that of mechanical stamping. (3) High energy, the single pulse energy of the laser beam can reach dozens of joules, and the peak power can reach GW. In the order of magnitude, the light energy is converted into shock wave mechanical energy within 10–20 ns, which realizes the efficient use of energy. In addition, LSP technique has outstanding advantages such as non-contact, no heat-affected zone, excellent controllability, and a significant strengthening effect.

However, the effects of LSP on mechanical behavior and microstructural response of 40CrMo steel are not clear. In view of this, 40CrMo steel was selected as the research object, the influence of LSP on the mechanical performance of 40CrMo steel and the micro-strengthening mechanism were explored.

2. Materials and Experiments

2.1. Materials

In this study, the used material was 40CrMo steel. The chemical composition and mechanical properties of the used 40CrMo steel are given in Tables 1 and 2.

Table 1. Chemical composition of the 40CrMo steel used in this study.

Elements	Cr	Mo	Si	Mn	C	Impurity	Fe
(Wt%)	1.35	0.25	0.25	0.55	0.38	≤0.07	Bal.

Table 2. Mechanical properties of 40CrMo steel.

Property	Value
Modulus of elasticity E (GPa)	206
Ultimate tensile strength σ_b (MPa)	1005
Tensile yield strength $\sigma_{0.2}$ (MPa)	425
Elongation at break δ (%)	12.5
Poisson's ratio	0.3

2.2. Laser Shock Peening Experiment

The LSP experiments were carried out with the Nd:YAG GAIA laser system. The main process parameters of the LSP experiments were as follows: the laser pulse width was 8 ns,

the wave length was 1064 nm, the laser energy was 8 J, the overlap rate was 50%, and the spot diameter was 3 mm. The absorption layer was aluminum foil with 0.12 mm thickness, and the constraining layer was a water curtain with about 2 mm thickness. The peening area and path of the samples used for surface integrity test are shown in Figure 1.

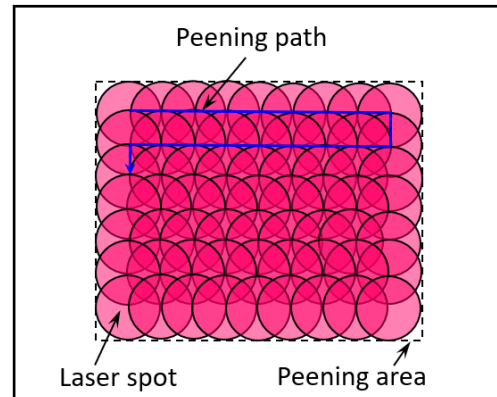


Figure 1. Schematic diagram of peening area and path.

2.3. Microhardness Measurement

The microhardness at depth direction of the specimens with and without LSP treatments was measured using an HV-1000 hardness tester (Yzjingmi Inc., Shanghai, China). During the process of the microhardness test, the used loading force and holding time were 10 N and 30 s, respectively. Five test points were selected on each treated sample to measure the microhardness value, and the five measurement results were averaged as the final microhardness value.

2.4. Tensile Properties Test

The tensile test at room temperature of the samples with and without LSP was carried out on a WDW-200G type electronic universal testing machine (Bainuo Inc., Shanghai, China). The device has a maximum loading force of 200 kN, and a tensile rate range of 0.005–500 mm/min, as well as a maximum tensile displacement of 700 mm. In this study, the tensile rate was 1 mm/min. The schematic of the tensile specimen size, LSP area and path is shown in Figure 2.

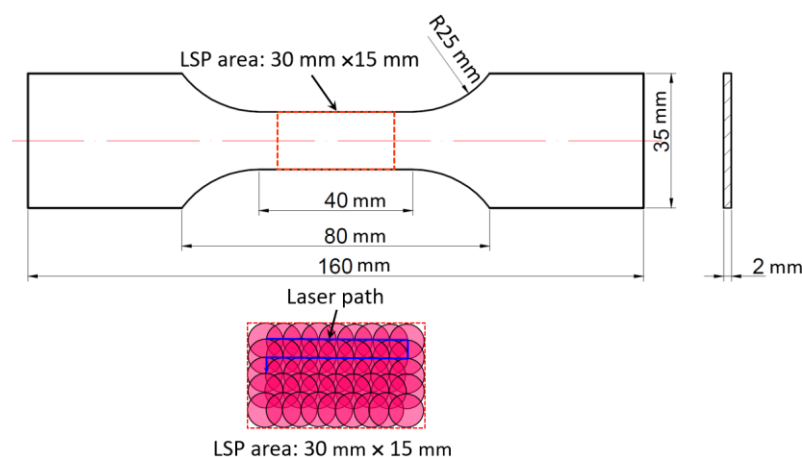


Figure 2. Schematic of tensile specimen dimensions, LSP area and path.

2.5. Residual Stress Test

The residual stress test was conducted with the X350 X-ray stress tester (AST Inc., Handan, China). The scan start angle was 149° , the scan end angle was 169° , and the scan step was 0.10° . The collimation tube diameter $\Phi = 1$ mm, the count interval was 1.0 s, the

target was Cr and the diffraction plane (hkl) was {211}. For the residual stress analysis, the test direction was parallel to the laser path. In order to test the residual stress in different depths of the sample after laser shock peening, a Struers LectrolPol-5 electrolytic polishing machine (Struers, Shanghai, China) was used to peel off the surface of the sample layer by layer. The residual stress value for each depth position was determined based on the average of five measured values. The test location for residual stress at the depth direction is shown in Figure 3.

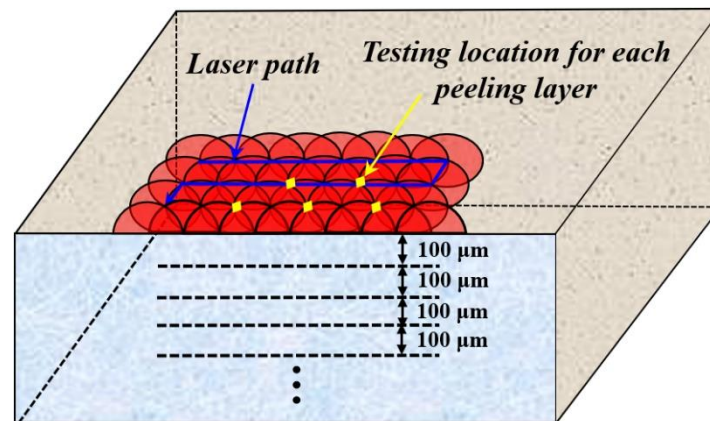


Figure 3. Test location for residual stress in the depth direction.

2.6. Microstructural Observation

In addition, the microstructure of the 40CrMo steel without and with LSP was observed by TECNAI G2 F20 TEM (FEI, Hillsboro, OR, USA). Firstly, the 40CrMo steel samples prepared for TEM observation were wire cut to 0.5 mm thickness, then polished to about 60 μm by mechanical grinding, and finally electronically thinned. Additionally, 5% perchloric acid and 95% ethanol was used to thin the sample. For each depth position, the zone for TEM observation is shown in Figure 4.

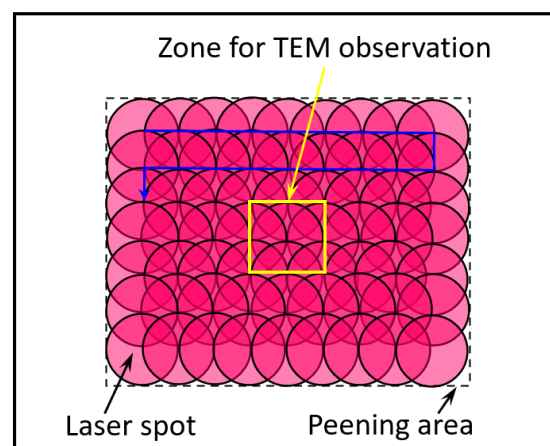


Figure 4. Zone for TEM observation at each depth position.

2.7. Wear Test

The CETR UMT-3 friction and wear tester (CETR, Bruck, Germany) were used to carry out the friction experiment. During the experiment, the grinding ball material was Si_3N_4 , and the wear mode was reciprocating mode. The friction load was 5 N, the experiment time was 30 min, and the relative sliding velocity was 0.025 m/s. Additionally, the size of the wear specimens before and after LSP treatment was 15 mm × 15 mm × 10 mm. After the experiment, the Sigma 500 scanning electron microscope (Oberkochen, Zeiss, Germany) was used to analyze the microscopic morphologies of the wear scar and the chemical composition of the debris.

3. Results and Discussion

3.1. In-Depth Residual Stress

In addition to the microstructure, the compressive stress introduced by LSP has an important influence on the mechanical properties of metal materials [15]. Meanwhile, the analysis on residual stress measured parallel to the laser path of 40CrMo steel without and with LSP treatments is also given in Figure 5. It was observed that there is a tensile stress of about 30 MPa on the surface of the original sample, which may be introduced by the pre-stretching process in the preparation of the 40CrMo steel. With the LSP process, the tensile stress of the 40CrMo steel was converted into compressive stress, and the surface compressive residual stress measured parallel to the laser path reached -425 MPa. When the shock wave pressure induced by laser exceeds the elastic limit of 40CrMo steel, the surface layer of the material undergoes plastic deformation. When the shock wave pressure is removed, the material in the deformed area will generate compressive residual stress in the plane perpendicular to the laser incident direction under the restriction and reaction of the surrounding materials. The in-depth compressive residual stress tested perpendicular to the laser path of the specimen continues to decrease with the increase of the distance from upper surface, until it drops to the level of the untreated sample. Furthermore, at a depth of $600\ \mu\text{m}$ the stress state of the specimen subjected to LSP is transformed from compressive stress to tensile stress, which illustrated the depth of the influence layer of laser shock peening on the residual stress of 40CrMo steel is about $600\ \mu\text{m}$.

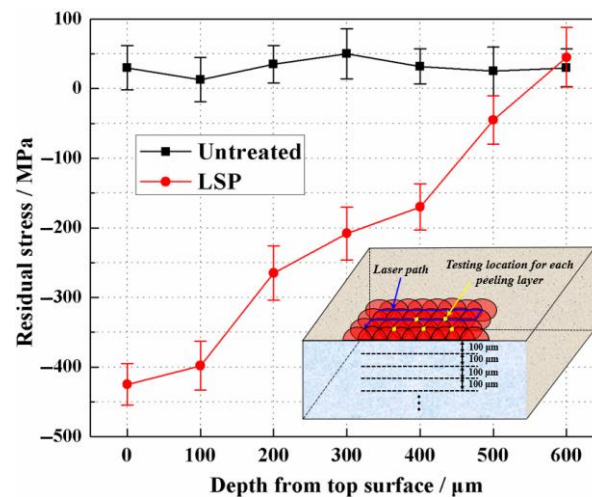


Figure 5. Gradient distribution of the residual stress measured parallel to the laser path of the samples without and with LSP treatments.

3.2. Microstructural Observation

To analyze the micro-strengthening mechanism of the LSP process on the mechanical behavior of 40CrMo steel, the microstructural evolution of the 40CrMo steel without and with LSP was characterized by TEM. Figure 6 presents the TEM images on the extreme surface of the original sample. It is observed that the black cementite lamellas are evenly distributed in the gray white ferrite matrix, and the grain boundaries were also clearly found. Meanwhile, a few dislocation structures were observed at the interfaces between ferrite and cementite. However, the dislocation density of the untreated sample is very low, and the dislocation structure is relatively dispersed.

Figure 7 displays the microstructures on the extreme surface treated by LSP. From Figure 7a, it is observed that the LSP process generated a high-density dislocation structure, while the high-density of dislocation structures were entangled with each other. From Figure 7b,c, LSP also induced a large number of deformation twins. The distance between adjacent deformation twins is approximately $300\ \mu\text{m}$. In addition, the deformation twins and dislocation structures were entangled and interacted with each other, as exhibited in Figure 7d. Figure 7e,f presents the selected-area electron diffraction (SAED) pattern

and the high-resolution TEM images on deformation twins in area A marked in Figure 7d. The observation results also imply a large number of dislocations distributed along the deformation twin boundaries. Meanwhile, the increase in dislocation density, the formation of deformation twins, and the interaction between twins and dislocations processed by LSP play a key role in enhancing the mechanical behavior of treated 40CrMo steel [16,17].

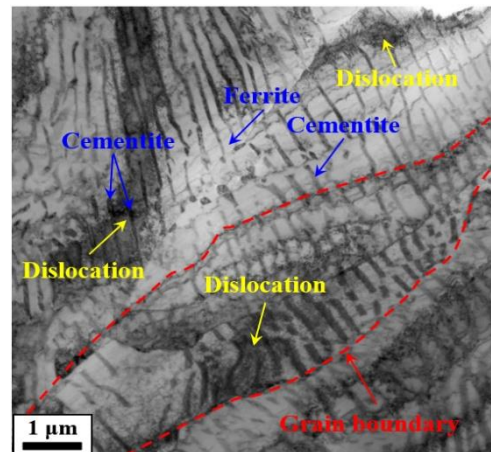


Figure 6. Microstructure characteristics on the extreme surface of the sample without LSP.

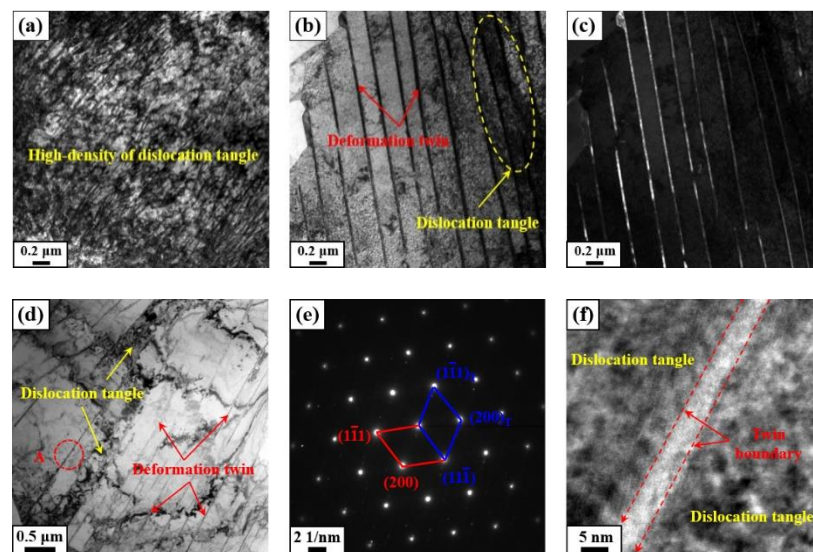


Figure 7. Microstructural TEM observation on the extreme surface treated by LSP. (a) High-density of dislocation tangle, (b,c) TEM bright-field image of deformation twin and its corresponding dark-field image, (d) Image of the interaction between deformation twin and dislocation, (e,f) SAED pattern and high-resolution TEM images on deformation twins in area A marked in (d).

Figure 8 shows the in-depth microstructural TEM observation in the near-surface layer of 40CrMo steel processed by LSP. It is noted that the severe plastic deformation promotes the precipitation of carbide particles (marked by the red circle) at a depth of 100 μm , and the pinning effect increases the dislocation density, as illustrated in Figure 8a. Additionally, the aggregation and expansion of dislocations form many dislocation cells and dislocation tangles, as demonstrated in Figure 8b,c. Meanwhile, the microstructures at a depth of 300 μm induced by the LSP process are given in Figure 8d,e. Many dislocation tangles and dislocation lines have been observed. Additionally, the TEM observation at a depth of 500 μm is shown in Figure 8f. The microstructure is mainly composed of a low-density of dislocation tangles, cementite and ferrite. During the propagation of the laser shock wave,

the energy continues to attenuate, which in turn causes a reduction in the degree of plastic deformation, finally causing a decrease in the dislocation density [18].

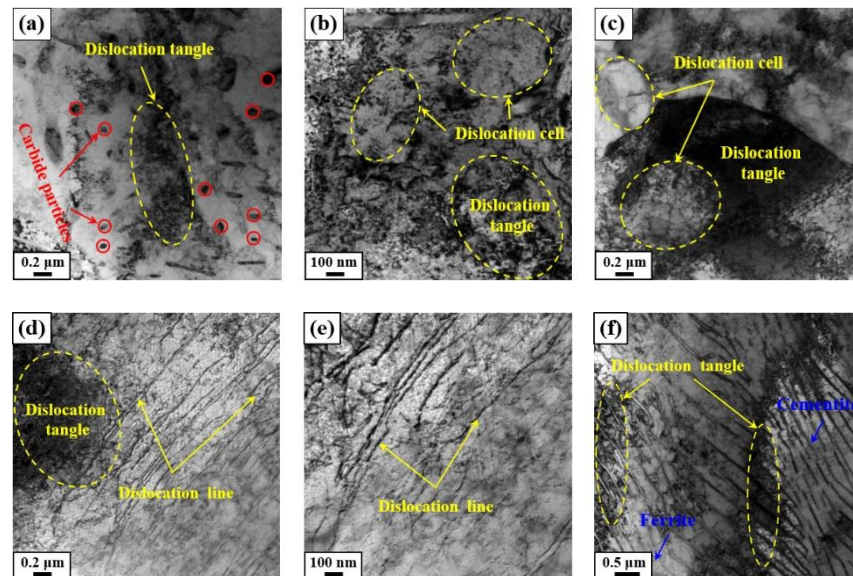


Figure 8. In-depth microstructural TEM observation in the near-surface layer of 40CrMo steel subjected to LSP. (a–c) at a depth of 100 μm , (d,e) at a depth of 300 μm , (f) at a depth of 500 μm .

3.3. In-Depth Microhardness

Figure 9 shows the comparison of the microhardness at depth direction of the samples without and with LSP. It is obvious that LSP treatment can effectively enhance the microhardness of the 40CrMo steel. Before the LSP process, the average surface microhardness of the specimen was about 278 HV, while LSP improved the surface microhardness value to 338 HV, which increased by 21.58%. Therefore, LSP treatment can effectively improve the surface microhardness of the 40CrMo steel. As the distance from the upper surface increases, the microhardness value of the sample continues to decrease, until it drops to the level of the untreated sample. Additionally, at a depth of 600 μm , the microhardness of the specimen is comparable to that of the untreated specimen, which also shows that the depth of the influence layer generated by laser shock peening on the microhardness of 40CrMo steel is about 600 μm . The higher surface hardness caused by LSP effectively hinders the initiation and propagation of cracks, which contributes to enhancing the mechanical properties of structural parts [19].

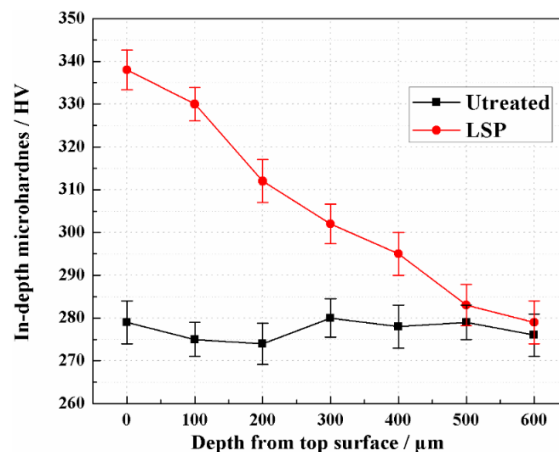


Figure 9. Microhardness at the depth direction of the samples without and with LSP.

3.4. Tensile Strength and Elongation

Figure 10 demonstrates the engineering stress-strain curves at room temperature of 40CrMo steel samples processed by different treatments. According to the tensile results, it is observed that the specimen subjected to LSP not only presents a high tensile strength, but also a high fracture plasticity. Meanwhile, the tensile strength and fracture elongation of the original specimen were 1005 (± 23) MPa and 12.5 (± 0.3)%, respectively. After LSP, the average tensile strength was increased by 15.9% from 1005 (± 23) MPa to 1165 (± 38) MPa. Moreover, the fracture elongation of the LSP specimen was 13.9 (± 0.5)%, which increased by 11.2% compared with the original sample. The deformation twin boundary can both prevent the movement of dislocations and provide the paths for dislocation slip, which can contribute to the simultaneous enhancement of strength and plasticity. Thus, the simultaneous improvement in tensile strength and plasticity of 40CrMo steel is mainly contributed to by the interaction of a high density of dislocations and deformation twins induced by LSP shown in Figure 7.

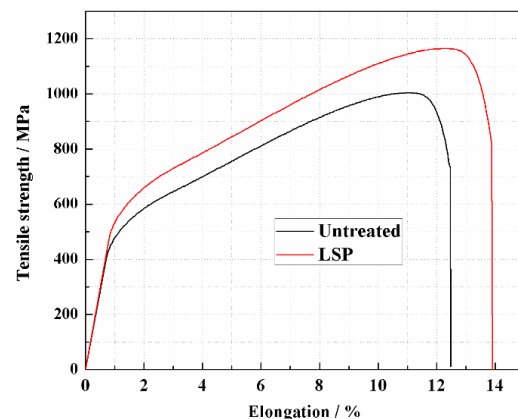


Figure 10. Engineering stress-strain curves of 40CrMo steel samples without and with LSP.

Figure 11 shows the tensile fracture morphologies of the samples with different treatments. The fracture morphologies characteristics of the two samples before and after LSP show the ductile fracture mode. However, it can be seen from Figure 11a,b that the dimples of the sample processed by LSP are larger and deeper. It also reflects that LSP can improve the plasticity of 40CrMo steel to a certain extent, which is consistent with the results shown in the tensile curve.

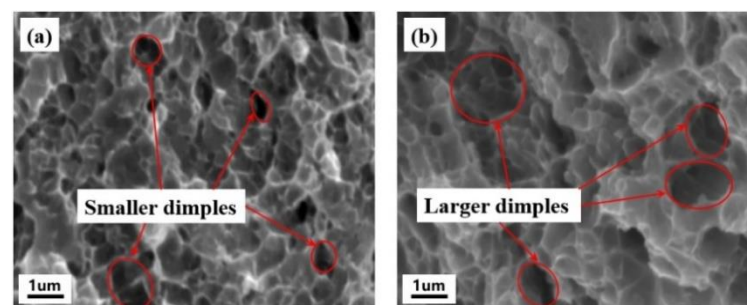


Figure 11. Tensile fracture morphologies of 40CrMo steel. (a) untreated sample and (b) LSP sample.

3.5. Wear Properties Analysis

After the wear tests, the mass loss of the specimens with and without LSP was measured. The comparison results show that the mass loss reduced after LSP treatments. After the wear tests, the mass loss of the original sample was about 167 mg, while that of the specimens treated by LSP was about 121 mg. After LSP treatment, the mass loss was reduced by 27.5% than that of the original specimen, which suggested that LSP could provide superior wear resistance.

To further analyze the wear behavior of 40CrMo steel subjected to the LSP process, the worn morphologies of 40CrMo steel specimens were also characterized by SEM, as illustrated in Figure 12. Figure 12a,b demonstrates the worn morphologies for the untreated sample, and Figure 12c,d demonstrates the worn morphologies for the sample treated by LSP. It is clear that the width of the wear scar of the original specimen is approximately 150 μm , while the value of the sample after LSP is about 105 μm . Additionally, there are some grooves on the worn surfaces of the samples, which were produced by micro plowing and micro cutting of abrasive. However, the grooves of the untreated samples are deeper and denser, while the grooves of the samples after LSP are slight. In addition, during the reciprocating wear process, adhesive scars and debris are produced along the direction of the wear scar. There were many debris particles on the untreated samples, and large areas of adhesives were also observed. Unlike the untreated sample, the adhesives on the worn surface of the sample subjected to LSP were hardly found. The analysis results show that the synergistic effect of microhardness improvement, compressive residual stress and beneficial microstructure generated by LSP significantly reduces the debris and adhesives of 40CrMo steel. LSP treatment changed the wear mechanism from adhesive wear and severe abrasive wear to slight grooves-like abrasive wear.

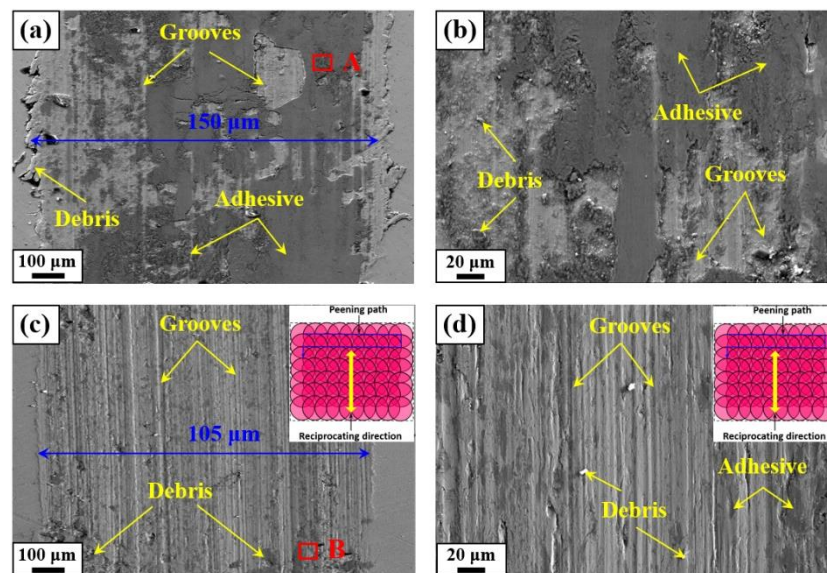


Figure 12. Worn micrographs on the surface of the differently processed samples. (a,b) untreated sample, (c,d) LSP sample.

In addition, an energy dispersive spectrometer (EDS) was used to detect the chemical composition of the debris, as shown in Figure 13. The EDS results of the debris in Figure 13a,b correspond to regions A and B shown in Figure 12, respectively. It can be seen that the chemical composition of the debris is Fe, Al and some impurity elements. However, there are some oxygen elements in the debris on the wear surface of the untreated sample, which is not conducive to the improvement of wear resistance. As shown in Figure 13b, there are some carbides on the worn surface of the laser shock peened sample, which can enhance the wear resistance of 40CrMo steel.

3.6. Discussion

3.6.1. Microstructural Evolution Mechanism

The process of microstructural response on 40CrMo steel generated by LSP treatment is mainly due to the intense severe plastic deformation. The high-intensity shock wave pressure will generate great amounts of interacting dislocation structures, causing the imbalance of system energy. The specific evolution process of the microstructure of 40CrMo steel is as follows.

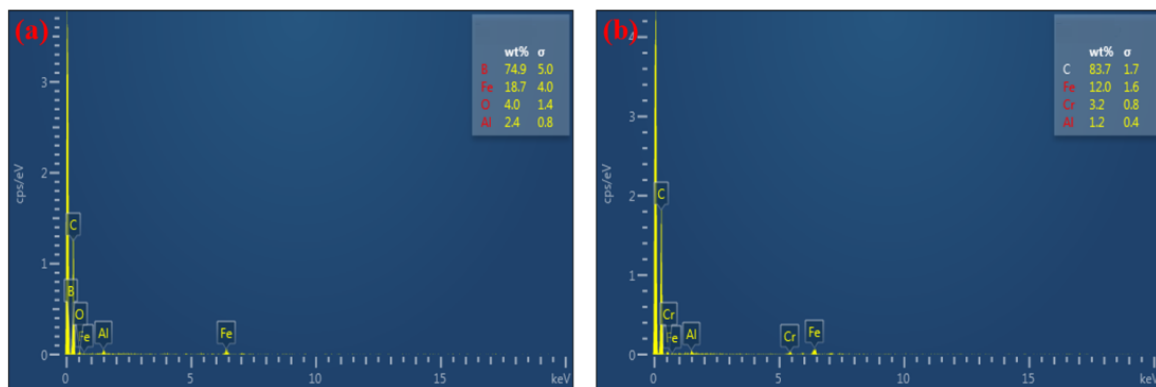


Figure 13. EDS analysis results of the debris in Figure 12. (a) corresponds to A area and (b) corresponds to B area.

During the process of the propagation of the laser shock wave, the severe plastic deformation induces large numbers of dislocation lines. Meanwhile, the continuous increase and aggregation of dislocation lines will form a complex dislocation structure, mainly including dislocation walls and dislocation networks. Then, the sub-grain boundaries will continue to absorb the accumulated dislocation structure and climbing in the grain, which increases the dislocation density near the sub-grain boundaries. With the migration and rotation of the sub-grain boundaries, part of the sub-grain boundaries continuously absorbs the surrounding dislocation structures, which causes the grain boundaries angle to increase continuously, and finally turns into low-angle grain boundaries. In addition, the low-angle grain boundaries continue to change to high-angle grain boundaries as the plastic deformation continues, which in turn leads to the refinement of the original structure [20,21].

Meanwhile, the lattice distortion caused by severe plastic deformation promotes the precipitation of carbides distributed in 40CrMo steel. The pinning effect of carbide inhibits the motion and slip of dislocations, and finally further improves the density and stability of dislocations [22]. When the dislocation density induced by LSP multiplies to a certain extent, the cross-slip of the dislocations is suppressed, the dislocation plugging is difficult to evolve into dislocation walls or sub-grain boundaries, and the dislocation plugging in the grain increases. The stress at the grain boundary cannot be released, and the accumulated energy cannot be released in time, which causes a greater stress concentration. Finally, the dislocations will continue to multiply with increasing deformation, and the density of dislocation distributed in more regions reaches saturation, which contributes to generating the deformation twin.

3.6.2. Wear Mechanism

Combined with the analysis results in Section 3.5, it is clear the wear model of 40CrMo steel during the friction process has changed from adhesive wear and severe abrasive wear to slight grooves-like abrasive wear after LSP. Because the grain refinement and the formation of twins can cause the increase of grain boundaries, which in turn hinder the movement of dislocations, the density and stability can be effectively improved [23]. Meanwhile, LSP introduces the precipitation of carbide particles into the surface layer of 40CrMo steel, shown in Figure 8a, which is beneficial to hinder the movement of dislocations in plastic deformation such as wear, and has a strengthening effect on pinning dislocations [24]. According to the Hall-Petch relationship, the improvement of dislocation density and grain refinement are beneficial to the improvement of the hardness of engineering materials [17]. Based on the measurement results of microhardness in Figure 9, the same conclusion is drawn. The high density of dislocations and deformation twins (shown in Figure 7) induced by LSP enhance the surface hardness of the 40CrMo steel. Generally speaking, the higher the hardness of the engineering material, the better the wear resistance [25,26].

Meanwhile, the high-amplitude of residual stress was formed at the surface direction tested parallel to the laser path and the depth direction test perpendicular to the laser path of the sample treated by LSP shown in Figure 5, which can offset the tensile stress caused by the wear process, thus increasing the wear resistance to a certain extent. Since the grain size of the sample is reduced after LSP, the size of the wear debris generated during the wear process is reduced, and no large pieces fall off, shown in Figure 12c,d, which is also a performance of the excellent wear resistance of the sample treated by LSP. In addition, the improvement in hardness, strength and plasticity caused by the formation of deformation twins and the dislocation proliferation play a critical role in enhancing the ability to resist wear of the 40CrMo steel. In view of the significant effect of laser shock peening technology on improving the mechanical properties of 40CrMo steel, the methodology can be also scaled up for industrial modification of steel.

4. Conclusions

The influence of LSP treatment on in-depth microhardness, tensile properties, and friction and wear properties of 40CrMo steel was explored. In addition, combined with the evolution of residual stress and microstructures, the micro-strengthening mechanism of LSP on 40CrMo steel was also explored. Some important findings are as follows.

- (1) After laser shock peening, the surface state of the specimen changed from tensile stress to compressive stress, and the surface compressive residual stress measured parallel to the laser path reached -425 MPa. Meanwhile, the surface microhardness was 338 HV, which increased by 21.58% compared with the original sample. According to the test results of residual stress and microhardness in the depth direction, it was judged that the depth of the influence layer of LSP was about 600 μm .
- (2) Laser shock peening caused severe plastic deformation on the surface layer of the processed sample, which induced the proliferation of dislocations, the formation of deformation twins and the precipitation of carbide particles, and thus contributed to increasing the mechanical properties of treated 40CrMo steel.
- (3) After laser shock peening, the tensile strength increased by 15.9% and the elongation increased by 11.2%. The deformation twin boundaries induced by laser shock peening can both prevent the movement of dislocations and provide the paths for dislocation slip, which can contribute to the simultaneous enhancement of strength and plasticity.
- (4) Compared to the original specimen, the mass loss of the sample subjected to laser shock peening treatment reduced by 6.40%. Additionally, LSP changed the wear mechanism of 40CrMo steel from adhesive wear and severe abrasive wear to slight grooves-like abrasive wear. The high microhardness, beneficial microstructure and high magnitude of compressive residual stress induced by LSP were beneficial to provide the specimen with excellent wear resistance.

Author Contributions: Conceptualization, H.Q.; Data curation, X.P., Z.G. and A.F.; Formal analysis, A.F. and J.L.; Investigation, X.P., Z.G., H.Q. and A.F.; Methodology, H.Q. and J.L.; Visualization, A.F.; Writing—original draft, X.P.; Writing—review & editing, X.P. All authors have read and agreed to the published version of the manuscript.

Funding: This research was supported by Zhejiang Provincial Natural Science Foundation of China under Grant No. LY20E050027.

Institutional Review Board Statement: Not applicable.

Informed Consent Statement: Not applicable.

Data Availability Statement: Not applicable.

Conflicts of Interest: The authors declare no conflict of interest.

References

1. Thuong, L.V.; Trung, D.D.; Chau, H.V.; Thuan, H.M.; Ke, D.Q. *Study on Plasma Nitriding Technology Imposed to Several Machine Parts Made of 40CrMo Steel*; Springer: Berlin/Heidelberg, Germany, 2014.
2. Thuong, L.V.; Trung, D.D.; Chau, H.V.; Thuan, H.M.; Ke, D.Q. Optimizing plasma nitriding regime of 40CrMo steel on Eltropol H045x080 device. *Vietnam. Mech. Eng. Mag.* **2012**, *6*, 62–69.
3. Wang, X.; Chen, J.-G.; Su, G.-F.; Li, H.-Y.; Wang, C. Plastic damage evolution in structural steel and its non-destructive evaluation. *J. Mater. Res. Technol.* **2020**, *9*, 1189–1199. [[CrossRef](#)]
4. Li, S.; Xie, X.; Cheng, C.; Tian, Q. A modified Coffin-Manson model for ultra-low cycle fatigue fracture of structural steels considering the effect of stress triaxiality. *Eng. Fract. Mech.* **2020**, *237*, 107223. [[CrossRef](#)]
5. Yang, Y.; Cui, X.; Zhao, X.; Dong, M.; Zhou, J.; Jin, G. Surface nanocrystallized structural steel with enhanced tribological properties under different sliding conditions. *Wear* **2020**, *460–461*, 203429. [[CrossRef](#)]
6. Sun, J.; Yang, C.; Guo, S.; Sun, X.; Ma, M.; Zhao, S.; Liu, Y. A novel process to obtain lamella structured low-carbon steel with bimodal grain size distribution for potentially improving mechanical property. *Mater. Sci. Eng. A* **2020**, *785*, 139339. [[CrossRef](#)]
7. Tsuchiya, S.; Takahashi, K. Improving fatigue limit and rendering defects harmless through laser peening in additive-manufactured maraging steel. *Metals* **2022**, *12*, 49. [[CrossRef](#)]
8. Cao, Y.; Wang, Z.; Shi, W.; Hua, G.; Qiu, M. Formation mechanism and weights analysis of residual stress holes in E690 high-strength steel by laser shock peening. *Coatings* **2022**, *12*, 285. [[CrossRef](#)]
9. Zhang, H.; Cai, Z.; Wan, Z.; Peng, P.; Zhang, H.; Sun, R.; Che, Z.; Guo, C.; Li, B.; Guo, W. Microstructure and mechanical properties of laser shock peened 38CrSi steel. *Mater. Sci. Eng. A* **2020**, *788*, 139486. [[CrossRef](#)]
10. Wang, J.; Lu, Y.; Zhou, D.; Sun, L.; Xie, L.; Wang, J. Mechanical properties and microstructural response of 2A14 aluminum alloy subjected to multiple laser shock peening impacts. *Vacuum* **2019**, *165*, 193–198. [[CrossRef](#)]
11. Liu, P.; Sun, S.; Xu, S.; Li, Y.; Ren, G. Microstructure and properties in the weld surface of friction stir welded 7050-T7451 aluminium alloys by laser shock peening. *Vacuum* **2018**, *152*, 25–29. [[CrossRef](#)]
12. Lan, L.; Jin, X.; Gao, S.; He, B.; Rong, Y. Microstructural evolution and stress state related to mechanical properties of electron beam melted Ti-6Al-4V alloy modified by laser shock peening. *J. Mater. Sci. Technol.* **2020**, *50*, 153–161. [[CrossRef](#)]
13. Wang, C.; Luo, K.; Bu, X.; Su, Y.; Cai, J.; Zhang, Q.; Lu, J. Laser shock peening-induced surface gradient stress distribution and extension mechanism in corrosion fatigue life of AISI 420 stainless steel. *Corros. Sci.* **2020**, *177*, 109027. [[CrossRef](#)]
14. Pant, B.; Pavan, A.; Prakash, R.V.; Kamaraj, M. Effect of laser peening and shot peening on fatigue striations during FCGR study of Ti6Al4V. *Int. J. Fatigue* **2016**, *93*, 38–50. [[CrossRef](#)]
15. Pavan, M.; Furfari, D.; Ahmad, B.; Gharghoury, M.; Fitzpatrick, M. Fatigue crack growth in a laser shock peened residual stress field. *Int. J. Fatigue* **2019**, *123*, 157–167. [[CrossRef](#)]
16. Lu, H.; Wang, Z.; Cai, J.; Xu, X.; Luo, K.; Wu, L.; Lu, J. Effects of laser shock peening on the hot corrosion behaviour of the selective laser melted Ti6Al4V titanium alloy. *Corros. Sci.* **2021**, *188*, 109558. [[CrossRef](#)]
17. Ye, C.; Suslov, S.; Lin, D.; Liao, Y.; Cheng, G.J. Cryogenic ultrahigh strain rate deformation induced hybrid nanotwinned microstructure for high strength and high ductility. *J. Appl. Phys.* **2014**, *115*, 213519. [[CrossRef](#)]
18. Liu, L.; Chi, R. Effect of microstructure on high cycle fatigue behavior of brass processed by laser shock peening. *Mater. Sci. Eng. A* **2018**, *740–741*, 342–352. [[CrossRef](#)]
19. Shi, X.; Feng, X.; Teng, J.; Zhang, K.; Zhou, L. Effect of laser shock peening on microstructure and fatigue properties of thin-wall welded Ti-6Al-4V alloy. *Vacuum* **2021**, *184*, 109986. [[CrossRef](#)]
20. Liu, H.; Hu, Y.; Wang, X.; Shen, Z.; Li, P.; Gu, C.; Du, D.; Guo, C. Grain refinement progress of pure titanium during laser shock forming (LSF) and mechanical property characterizations with nanoindentation. *Mater. Sci. Eng. A* **2013**, *564*, 13–21. [[CrossRef](#)]
21. Lu, J.; Luo, K.; Zhang, Y.; Sun, G.; Gu, Y.; Zhou, J.; Ren, X.; Zhang, X.; Zhang, L.; Chen, K.; et al. Grain refinement mechanism of multiple laser shock processing impacts on ANSI 304 stainless steel. *Acta Mater.* **2010**, *58*, 5354–5362. [[CrossRef](#)]
22. Ye, C.; Suslov, S.; Kim, B.J.; Stach, E.A.; Cheng, G.J. Fatigue performance improvement in AISI 4140 steel by dynamic strain aging and dynamic precipitation during warm laser shock peening. *Acta Mater.* **2011**, *59*, 1014–1025. [[CrossRef](#)]
23. Gu, K.; Zhang, H.; Zhao, B.; Wang, J.; Zhou, Y.; Li, Z. Effect of cryogenic treatment and aging treatment on the tensile properties and microstructure of Ti-6Al-4V alloy. *Mater. Sci. Eng. A* **2013**, *584*, 170–176. [[CrossRef](#)]
24. Li, G.; Cheng, J.; Wang, H.; Li, C. The influence of cryogenic-aging circular treatment on the microstructure and properties of aluminum matrix composites. *J. Alloy. Compd.* **2017**, *695*, 1930–1945. [[CrossRef](#)]
25. Wang, H.; Kalchev, Y.; Wang, H.; Yan, K.; Gurevich, E.; Ostendorf, A. Surface modification of NiTi alloy by ultrashort pulsed laser shock peening. *Surf. Coatings Technol.* **2020**, *394*, 125899. [[CrossRef](#)]
26. Lin, Y.; Cai, Z.-B.; Li, Z.-Y.; Yin, M.-G.; Wang, W.-J.; He, W.-F.; Zhou, Z.-R. Study on the abrasive wear behavior of laser shock peening Ti-6Al-4V titanium alloy under controlled cycling impact. *Wear* **2019**, *426–427*, 112–121. [[CrossRef](#)]